Supplemental material for 'Structure-Property relations of silicon oxycarbides studied using a machine learning interatomic potential'

Niklas Leimeroth, Jochen Rohrer, Karsten Albe

March 15, 2024

S1 Steady state of glassy structure

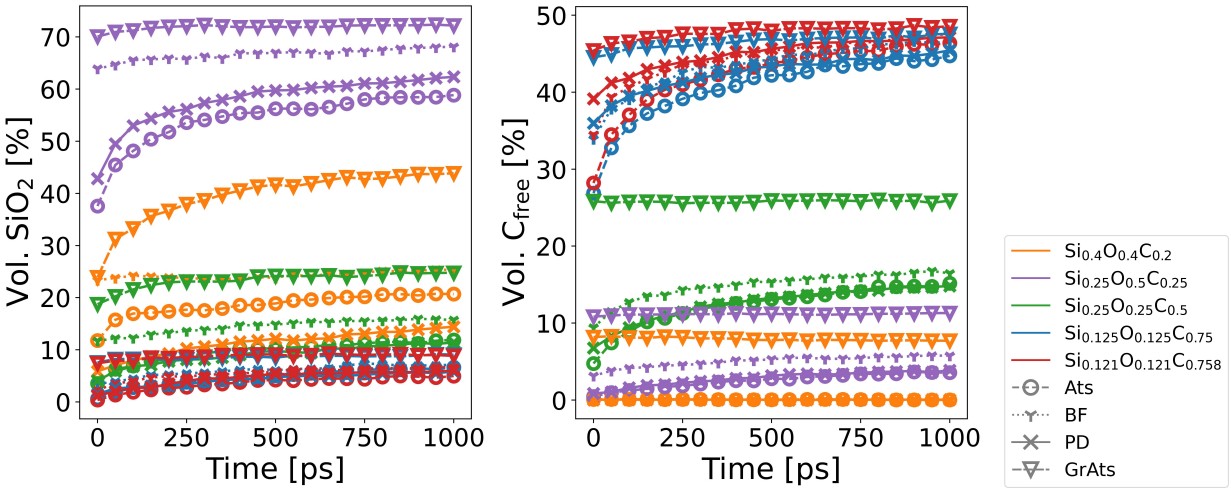

Figure S1: Volume fraction of SiO_4 tetrahedra and free carbon while equilibrating at 2000 K.

Fig. S1 shows volume fractions of structural features while equilibrating the structures during cook and quench simulations. After 1 ns the structural features do not undergo major changes anymore.

S2 Distribution of training data

The distribution of structures with respect to their number of atoms, atomic volume, formation energy distance from the convex hull and maximum force are shown in Fig. S2.

S3 Si centered tetrahedra

Fractions of different SiO_xC_{4-x} tetrahedra for the samples used in this work are shown in Fig. S3-S7. Generally values differ significantly depending on the temperature and building blocks used to generate the structures.
The plots also include experimental values measured with ^{29}Si CPMAS NMR (dashed horizontal lines) and Hahn-echo ^{29}Si MAS NMR (dotted horizontal lines), taken from [1]. Please note that the experimental samples have significantly different compositions than the simulated ones, because

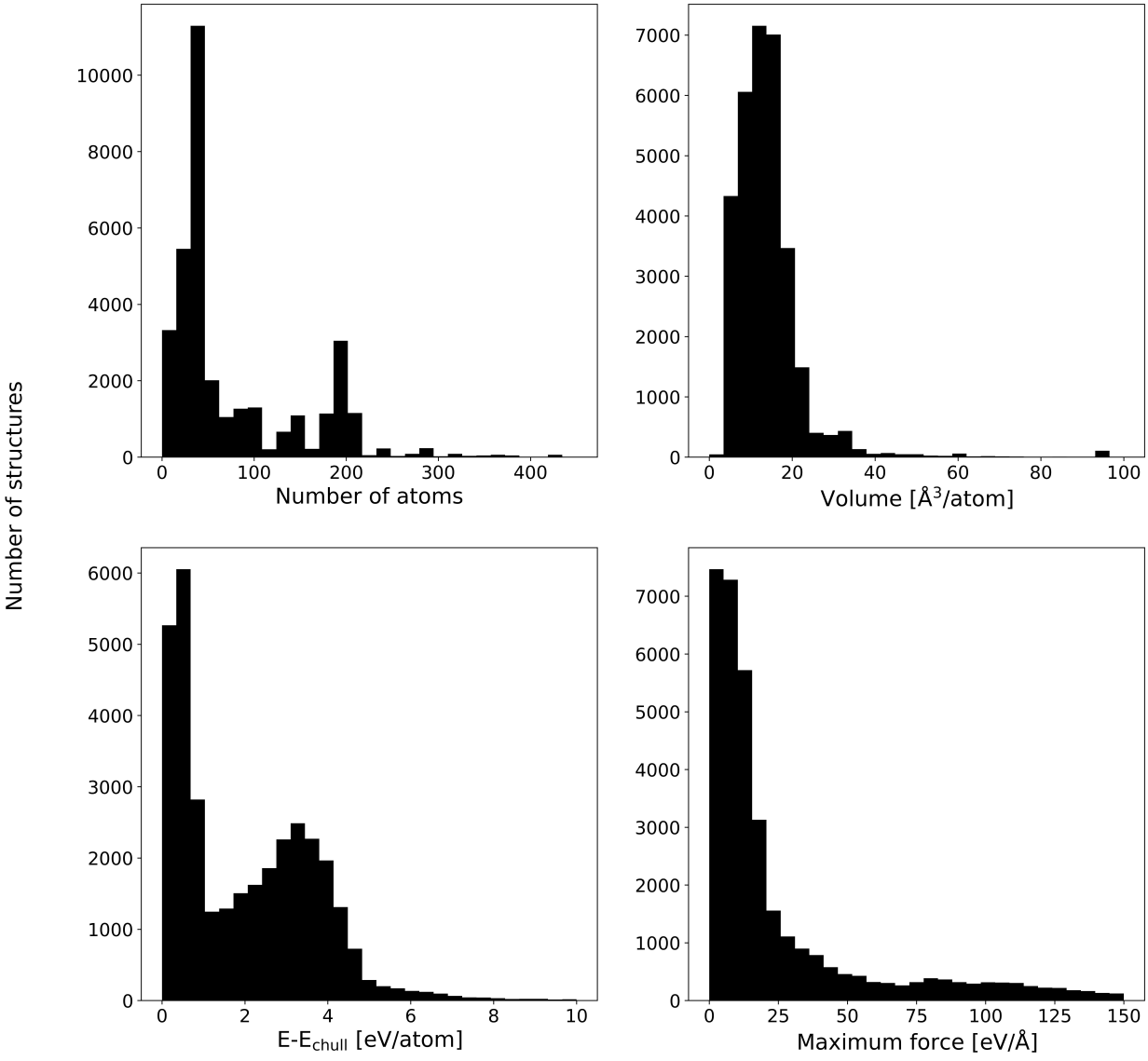

Figure S2: Properties of training data employed in the main work. The dataset also contains some surface structures, which were created by adding vacuum around existing structures. The histogram of atomic volumes is cutoff at $100\,\text{Å}^3$ to show details of the bulk samples, so they are not included.

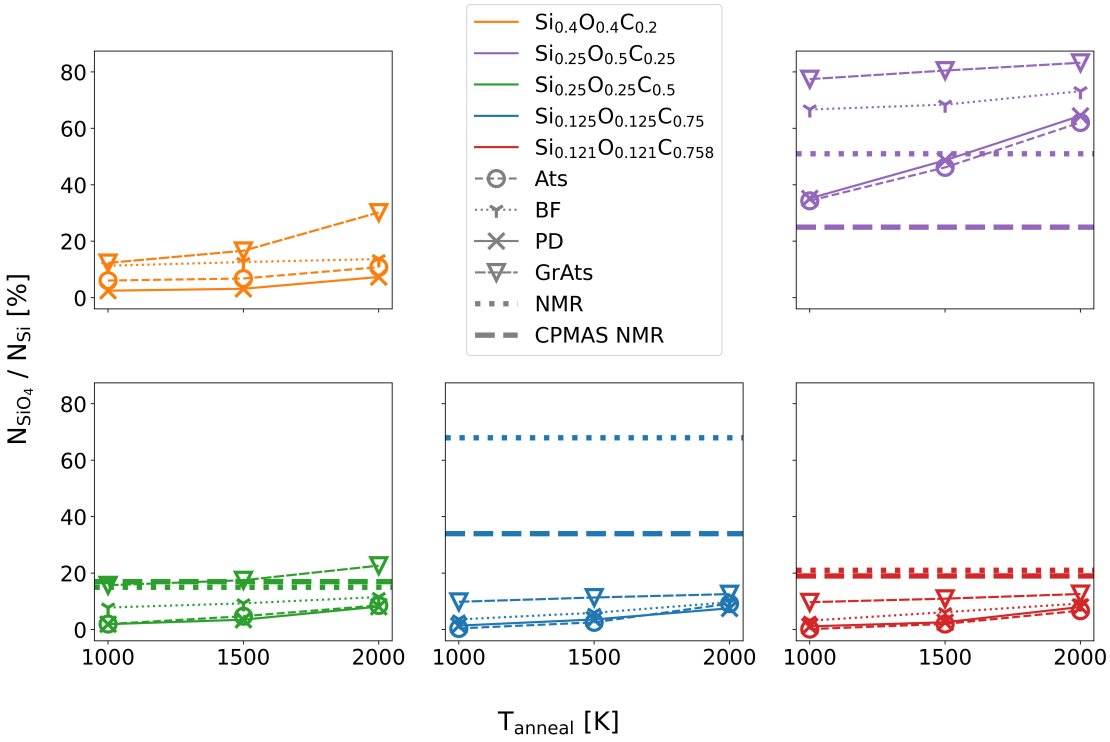

Figure S3: See text for more information.

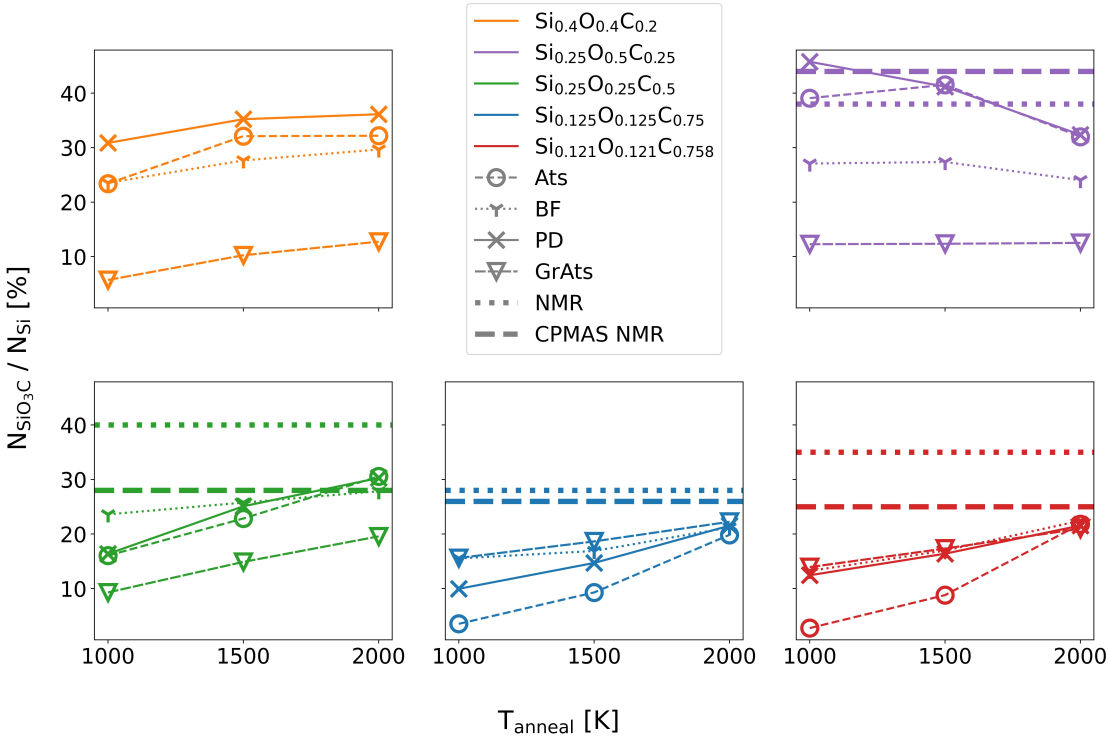

Figure S4: See text for more information

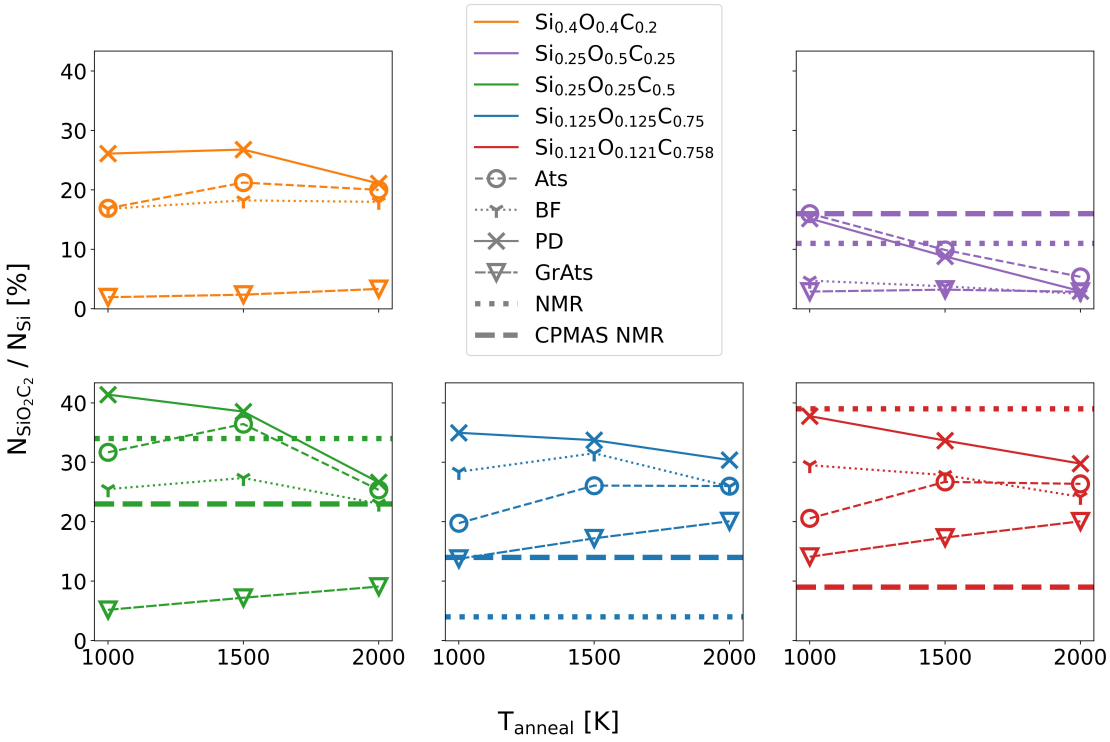

Figure S5: See text for more information

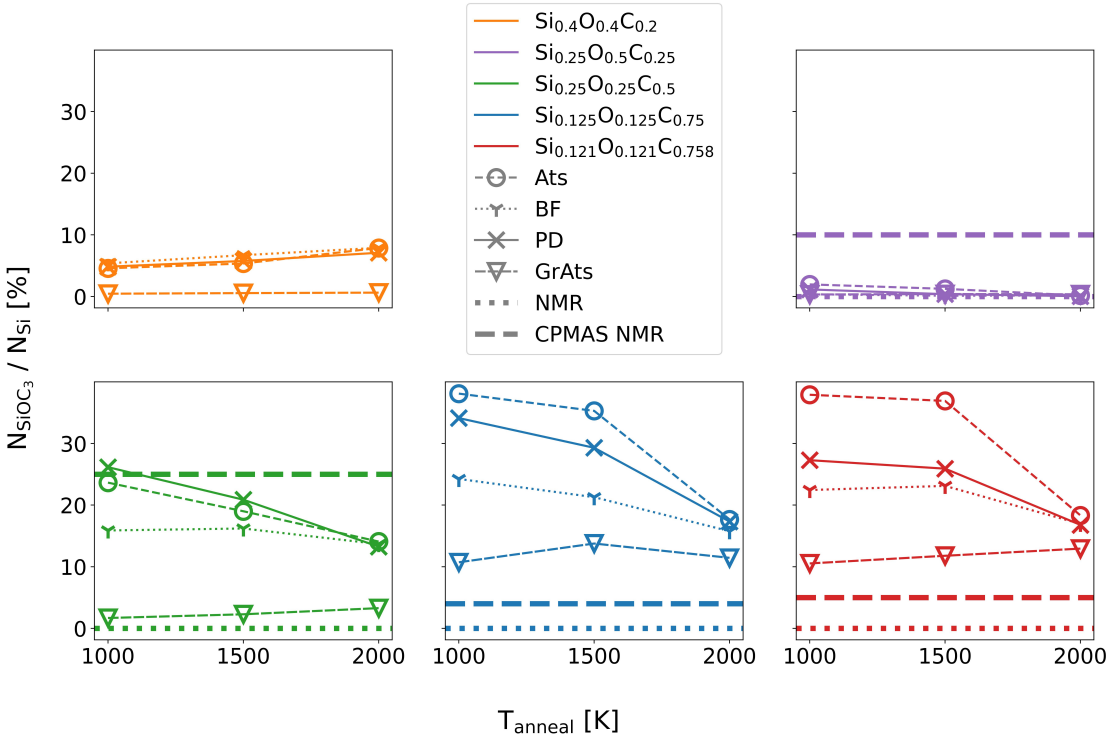

Figure S6: See text for more information

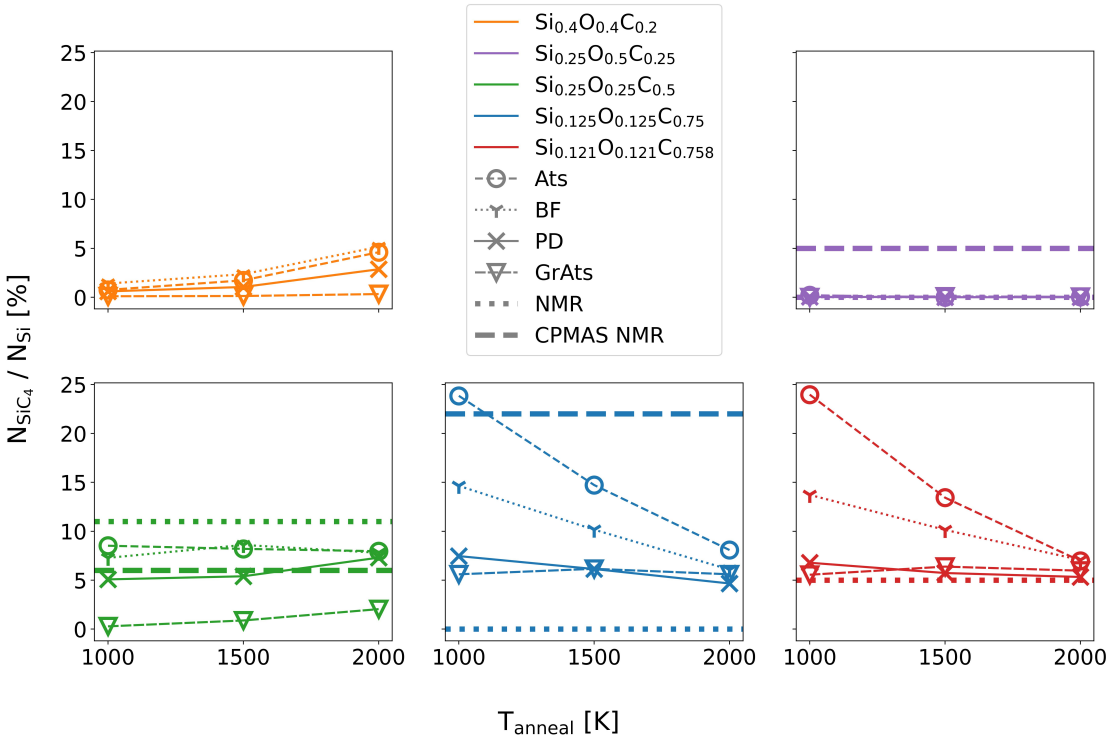

Figure S7: See text for more information

several gaseous products can evaporate during the polymer based synthesis route. The SiO_4 and SiO_3C fractions are typically slightly underestimated. For SiO_2C_2 and SiC_4 the agreement is better, while $SiOC_3$ is overestimated especially for the carbon rich structures with SILRES604 and RD684 composition. A major reason for these differences is presumably the already mentioned difference in compositions in combination with the short time scales achievable in MD simulations.

S4 Young's modulus from elastic tensor

Figures S8 to S9 show the strain-energy relation of the 6 applied strain states for a subset of structures and expected approximately harmonic behavior. The elastic tensors are calculated by the linear strain-stress relation.

S5 Speed of ReaxFF and ACE

The computational cost of the fitted ACE potential and an exemplary ReaxFF potential [2] is about the same order of magnitude as shown in Fig. S12. For the evaluation of the runtime the LAMMPS code was employed to simulate an SiOC structure with 80896 atoms on a single core of AMD Ryzen 5800X processor and an NVIDIA RTX 3060 GPU respectively.
In this example the fitted ACE potential is slightly faster than the ReaxFF. However, we want to note that the runtime of ACE potentials massively depends on the amount of basis functions used in the fit. Similarly, the runtime of the ReaxFF potential depends on the frequency with which charges are equilibrated and the employed cutoff, so other tests could show both potentials significantly faster or slower.

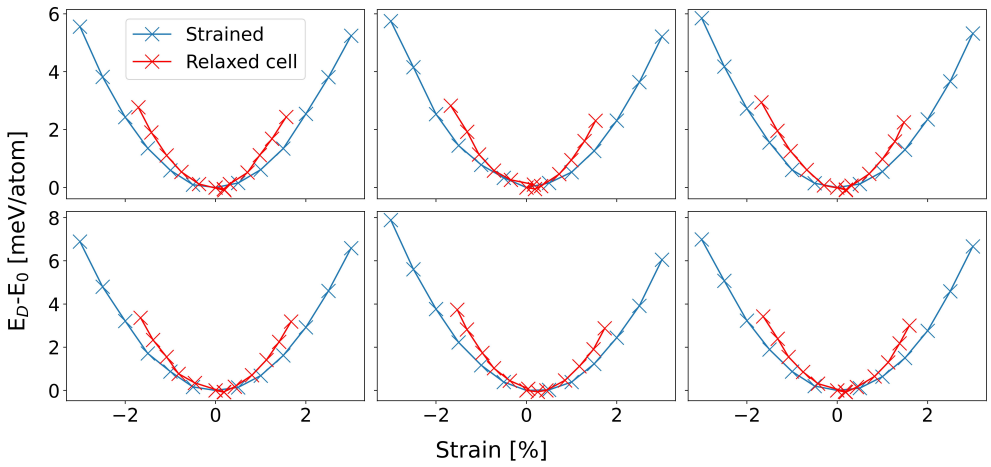

Figure S8: Strain-energy relation of Si_2O_2C structure based on single atoms.

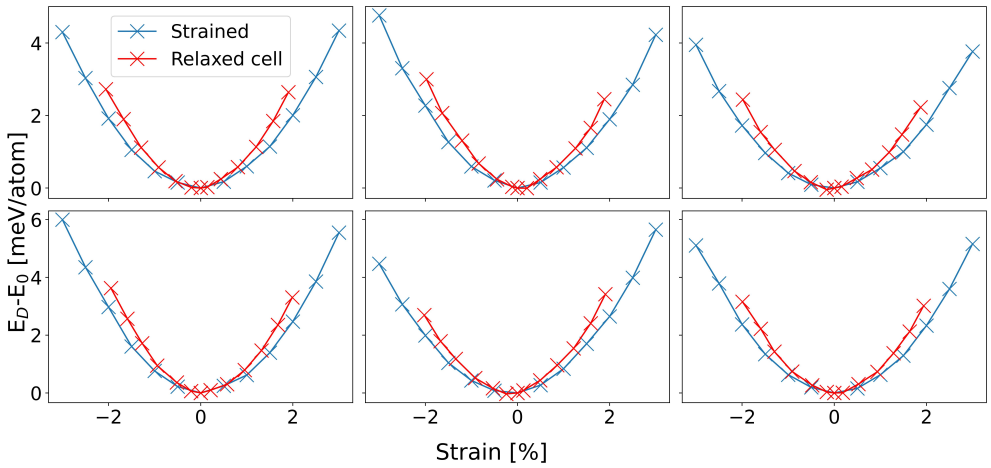

Figure S9: Strain-energy relation of PMSQ structure based on graphite and atoms.

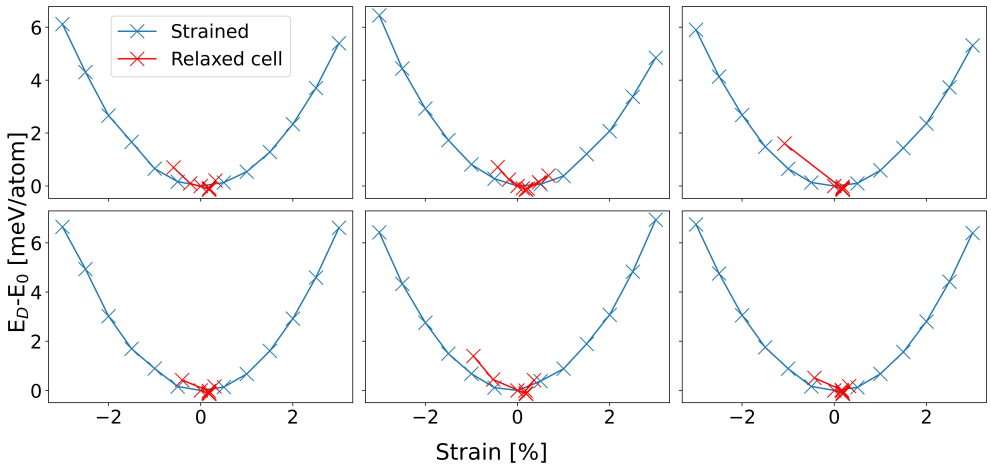

Figure S10: Strain-energy relation of RD-212 structure based on H-stripped polymers.

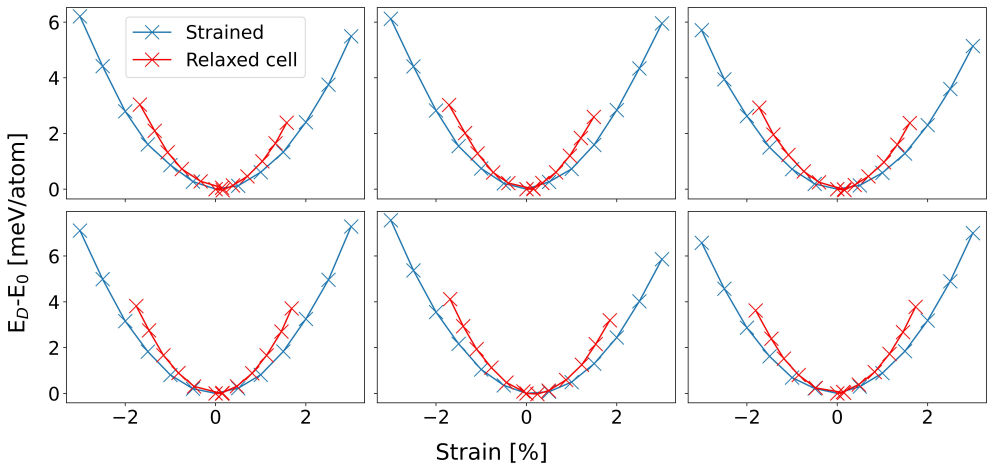

Figure S11: Strain-energy relation of SILRES-604 structure based on molecules.

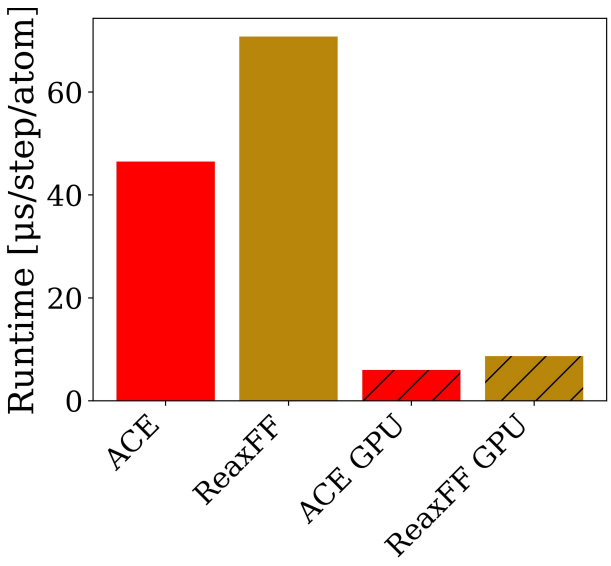

Figure S12: The computational costs of Atomic Cluster Expansion (ACE) and ReaxFF potentials are about the same order of magnitude. See text for details.